STATISTICS, OPTIMIZATION AND INFORMATION COMPUTING
Stat., Optim. Inf. Comput., Vol. **14**, September 2025, pp 1337–1355.
Published online in International Academic Press (www.IAPress.org)

Comparative Analysis of Control Strategies for Single-Phase PWM-CSCs Feeding Linear Loads: IDA-PBC, Nonlinear PI, and PI-PBC

Angélica Mercedes Nivia-Vargas [1], Oscar Danilo Montoya [2], Walter Gil-Gonzalez [3]

[1] *Doctoral student in Engineering, Universidad Distrital Francisco José de Caldas, Bogotá, Colombia*
[2] *Facultad de Ingeniería, Universidad Distrital Francisco José de Caldas, Bogotá D.C. 110121, Colombia*
[3] *Department of Electrical Engineering, Universidad Tecnológica de Pereira, Pereira, Colombia*

Abstract This study provides an in-depth analysis and a comparison of control strategies for single-phase pulse width modulation current source converters (PWM-CSCs) feeding linear loads, with a focus on the implementation of interconnection and damping assignment passivity-based control (IDA-PBC), nonlinear proportional-integral (PI) control, and passivity-based PI control (PI-PBC). The dynamic characterization of PWM-CSC systems is examined through state variables, including inductor current and capacitor voltage, to accurately model system behavior. The Lyapunov stability theorem ensures the global asymptotic stability of the equilibrium points, demonstrating that the proposed control techniques effectively drive system states to their desired values over time. The simulation results, obtained using the MATLAB environment, illustrate the performance of the proposed controllers. These results show that the controllers minimize the total harmonic distortion (THD) while maintaining a stable output current regulation. Furthermore, both IDA-PBC and PI-PBC exhibit superior performance in terms of stability and signal fidelity when compared to nonlinear PI control. This study not only advances the theoretical understanding of PWM-CSC control but also offers practical insights into the implementation of the aforementioned controllers in renewable energy systems and industrial applications. In addition, this paper proposes future research directions to further enhance the existing control strategies for PWM-CSCs.

Keywords Single-phase current source converter, linear loads, passivity-based control, IDA-PBC, PI-PBC, nonlinear PI control, total harmonic distortion, Lyapunov stability.

DOI: 10.19139/soic-2310-5070-2410

Nomenclature

Acronyms

IDA-PBC Interconnection and damping assignment passivity-based control

IGBT Insulated gate bipolar transistors

pH port-Hamiltonian

PI Proportional-integral

PI-PBC Proportional-integral passivity-based control

PWM-CSC Pulse-width modulation current-source converter

*Correspondence to: O. D. Montoya (Email: odmontoyag@udistrital.edu.co). Facultad de Ingeniería, Universidad Distrital Francisco José de Caldas, Bogotá D.C. 110121, Colombia

ISSN 2310-5070 (online) ISSN 2311-004X (print)

THD Total harmonic distortion

Parameters

$\mathcal{D}$ Energy storage array

$\mathcal{J}$ Skew-symmetric interconnection matrix

$\mathcal{R}$ Dissipation matrix

$\mathcal{V}(x)$ Lyapunov function

$\tilde{x}_1$ Error of x_1

$\tilde{x}_2$ Error of x_2

ϑ External inputs vector

C_o Capacitor value on the AC side (F)

G_L Linear load conductance (S)

I_h Harmonic ripple amplitude (A)

I_s DC component of x_1 (A)

k_i Integral constant

k_p Proportional constant

L_i Inductor value on the DC side (H)

m Modulation index

r_i Series-modeled coil resistance on the DC side (Ω)

R_L Linear load on the AC side (Ω)

u Control signal

$u^\star$ Smooth control input for maintaining the system's desired behavior

V_i DC input voltage source (V)

x_1 State variable representing the inductor current i_i (A)

x_2 State variable representing the voltage capacitor v_o (V)

$x_1^\star$ Desired operating point of x_1

$x_2^\star$ Desired operating point of x_2

1. Introduction

Pulse width modulation current-source converters (PWM-CSCs) have emerged as a suitable technology for regulating the output current of systems with variable or uncertain input voltage. These devices are widely used in applications such as power supplies, renewable energy systems, and electric vehicles, where the ability to maintain a stable output current despite input voltage variations is critical [3]. These converters work by modulating the width of pulses to control the current through an inductor, providing a versatile and efficient power conversion solution [2]. However, achieving high performance and stability in these systems requires implementing advanced control strategies that ensure reliable operation under dynamic conditions. This study focuses on the design and comparative analysis of several control techniques, including interconnection and damping assignment passivity-based control (IDA-PBC) and nonlinear proportional-integral (PI) control.

The PBC approach, based on passive systems theory, has been widely studied in the field of power electronics and control systems [17]. PBC exploits the inherent energy structure of the system to design controllers that ensure stability, robustness, and an energy-efficient operation [9]. In particular, IDA-PBC assigns damping and coupling terms to ensure that the system behaves passively and the states converge to the desired equilibrium points [5]. These features are particularly valuable for PWM-CSCs, which exhibit inherently nonlinear dynamics due to the switching nature of the converter.

Nonlinear controllers (*e.g.*, the nonlinear PI controller) offer an alternative to traditional linear control schemes by incorporating nonlinearities into the control law [20]. They are designed to improve performance in systems with complex dynamics, such as those found in power electronics, where linear models may not capture all the essential behaviors. Nonlinear PI controllers have been shown to improve performance in terms of transient response and stability when compared to their linear counterparts, making them an attractive option for PWM-CSC applications [27].

The theoretical foundation of this research corresponds to the dynamic characterization of PWM-CSCs, where state variables such as the inductor current and capacitor voltage are used to model the behavior of the system. These state-space models describe how the converter responds to changes in control inputs, such as modulation signals, and how the internal dynamics evolve [11]. To ensure that the system remains stable and reaches its desired operating point, the Lyapunov stability criterion is used. According to this principle, a system is stable if there is a Lyapunov function whose time derivative is negative-definite, ensuring that the states of the system asymptotically converge to a desired equilibrium point [21]. This method is particularly useful for analyzing the stability of nonlinear systems such as PWM-CSCs, where traditional linear stability analysis may not be applicable.

In this work, the implementation of the aforementioned control strategies is evaluated through simulations performed in the MATLAB environment. These simulations model the behavior of PWM-CSCs under different operating conditions and different control inputs. The effectiveness of each control approach is evaluated through key performance metrics such as voltage and current tracking accuracy, total harmonic distortion (THD) reduction, steady-state error, and settling time. The results provide a comprehensive understanding of how each control method affects the overall performance and stability of the PWM-CSC, providing insight into its practical applicability for different types of power conversion systems.

1.1. Contributions

This study makes valuable contributions to the field of control for PWM-CSCs. Firstly, it provides a comprehensive comparison of three control techniques: IDA-PBC, PI-PBC, and nonlinear PI control. Through an analysis of their corresponding strategies, this work identifies the advantages and disadvantages of these controllers in terms of reference tracking, stability, and THD, thus providing a valuable framework for selecting the most suitable control method for specific applications [25]. Moreover, the research employs dynamical models based on Hamiltonian theory to describe the behavior of PWM-CSC systems, offering a deeper understanding of system dynamics and a robust foundation for designing controllers that guarantee Lyapunov stability [18].

Moreover, this study presents comprehensive simulation results that attest to the efficacy of the proposed control techniques. IDA-PBC and PI-PBC achieved a significantly lower THD, demonstrating their ability to maintain high signal fidelity in comparison with the nonlinear PI controller. Notably, the system was designed and evaluated for

linear loads, further validating the controllers' effectiveness under such conditions. The findings have practical implications for the implementation of these controllers in renewable energy systems, electric vehicles, and other industrial applications where precise current regulation and harmonic distortion minimization are crucial. Furthermore, this work lays foundations for future research, suggesting potential avenues for the development of new control strategies aimed at further enhancing the performance of PWM-CSC systems in diverse operational conditions.

1.2. Document structure

This document is structured to facilitate the comprehension of its concepts and results. Section 1 provides an overview of the topic, examines the significance of PWM-CSCs, and outlines the objectives of the study. This section establishes the context for the research and identifies the control techniques to be analyzed. Section 2 presents the electrical configuration of a PWM-CSC, analyzes its operating principles, and introduces the dynamical models that govern its behavior, along with the relevant state variables. Section 4 describes the nonlinear control techniques employed in this study, including IDA-PBC, PI-PBC, and the nonlinear PI controller. This section also discusses the design parameters and methodologies associated with each technique.

Section 4 presents the simulation results for each control technique, providing an analysis of the data, a comparison of the controllers' performance, and a discussion of the implications of the results obtained in terms of reference tracking and harmonic distortion. Finally, Section 5 summarizes the key findings, discusses the contributions made, and suggests directions for future research in the field of converter control. The document concludes with a reference section that lists the sources and prior studies that support the research.

2. Dynamic characterization of a PWM-CSC feeding a linear load

Figure 1 presents the electrical configuration of the PWM-CSC analyzed in this study. This topology leverages electronically controlled switches, such as IGBTs, to achieve independent control of the output current regardless of the input voltage. Thus, the magnitude and direction of the output current can be accurately regulated [28]. The modulation process is governed by a pulse width modulation (PWM) strategy that generates switching signals based on a modulation index m.

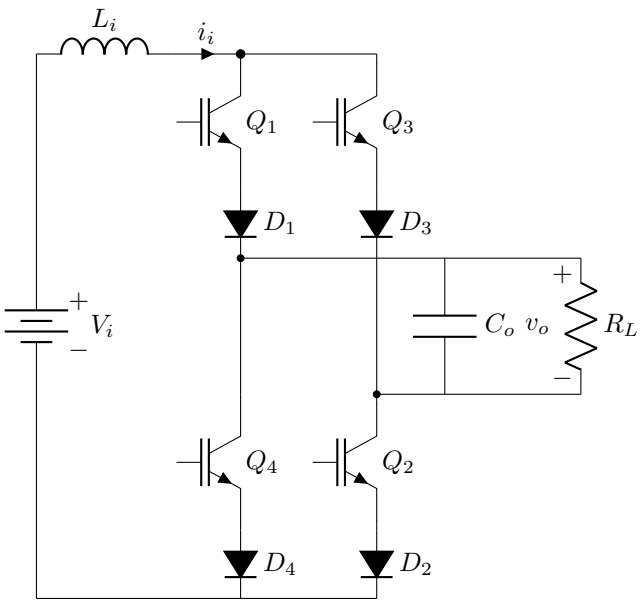

Figure 1. Configuration of the studied PWM-CSC

To minimize harmonic distortion, the system incorporates an output filter. This filter, which includes the capacitor C_o, is designed to effectively absorb harmonic currents. The system's dynamic behavior is characterized using two state variables: the inductor current (i_i) and the capacitor voltage (v_o). Applying Kirchhoff's circuit laws yields the following differential equations:

$$L_i \frac{di_i}{dt} = V_i - r_i i_i - m v_o, \tag{1}$$

$$C_o \frac{dv_o}{dt} = m i_i - G_L v_o. \tag{2}$$

In this setup, V_i represents the DC input voltage source, and L_i corresponds to the boosting inductor that attenuates the high-frequency harmonics generated during the switching process. The inductor model also accounts for a series resistance r_i. Furthermore, the load is represented by an equivalent conductance G_L, defined as $G_L = \frac{1}{R_L}$.

When expressed in terms of the state variables x_1 and x_2, the system is represented as follows:

$$L_i \dot{x}_1 = V_i - r_i x_1 - u x_2, \tag{3}$$

$$C_o \dot{x}_2 = u x_1 - G_L x_2. \tag{4}$$

The dynamical model expressed in Equations 3 and 4 can be reformulated as a port-Hamiltonian (pH) structure [4]:

$$\begin{bmatrix} L_i & 0 \\ 0 & C_o \end{bmatrix} \begin{bmatrix} \dot{x}_1 \\ \dot{x}_2 \end{bmatrix} = \left(\begin{bmatrix} 0 & -u \\ u & 0 \end{bmatrix} - \begin{bmatrix} r_i & 0 \\ 0 & G_L \end{bmatrix} \right) \begin{bmatrix} x_1 \\ x_2 \end{bmatrix} + \begin{bmatrix} V_i \\ 0 \end{bmatrix}, \tag{5}$$

$$\mathcal{D}\dot{x} = (\mathcal{J}(u) - \mathcal{R})\, x + \vartheta, \tag{6}$$

In this formulation, the matrix $\mathcal{D}$ represents the energy storage properties of the system, while $\mathcal{J}(u)$ corresponds to the interconnection matrix. Notably, $\mathcal{J}(u)$ is skew-symmetric, satisfying the condition $\mathcal{J}(u) + \mathcal{J}^\top(u) = 0$. The matrix $\mathcal{R}$ encompasses the dissipation effects within the system, and ϑ denotes the vector of external inputs [15]. By comparing Equations (5) and (6), the explicit forms of $\mathcal{D}$, $\mathcal{J}$, $\mathcal{R}$, and ϑ can be deduced [23].

Within this framework, the matrix $\mathcal{D}$ characterizes the energy storage properties of the system, while $\mathcal{J}(u)$ is the interconnection matrix, which is skew-symmetric and satisfies $\mathcal{J}(u) + \mathcal{J}^\top(u) = 0$. The dissipation effects are contained in the matrix $\mathcal{R}$, and ϑ denotes the vector of external inputs. By comparing Equations (5) and (6), the explicit forms of $\mathcal{D}$, $\mathcal{J}$, $\mathcal{R}$, and ϑ can be determined.

The central attribute of the dynamical model described in Equation 6 is that it enables the design of a nonlinear feedback controller grounded in passivity principles. This methodology ensures closed-loop stability in the sense of Lyapunov. To this effect, the desired dynamics must be appropriately selected in order to preserve the pH properties of the system, as discussed in [13].

3. Nonlinear control techniques

This section details the key components of the proposed control framework. Firstly, the desired operating point is introduced, with a description of the methodology for determining feasible trajectories for the state variables based on the system's dynamical model. The mathematical formulation of the desired trajectory is thoroughly developed, including its state-space equations and control input expressions, in order to lay the foundations for the nonlinear control design. Additionally, the derivation of critical parameters and the verification of equilibrium conditions are discussed, aiming to ensure system consistency.

The IDA-PBC design is then presented, along with the nonlinear control technique that leverages passivity theory and the Hamiltonian structure used to stabilize the system. Afterwards, this section elaborates on the

design of interconnection and dissipation matrices, the derivation of the error dynamics, and the formulation of the control law. The PI-PBC design is also explained, with an emphasis on the integration of proportional and integral components into the passivity-based approach to enhance stability and performance. Finally, the nonlinear PI control strategy is detailed, describing the incorporation of nonlinear proportional and integral components to address system uncertainties and improve the dynamic response. A stability analysis using Lyapunov theory and the incremental model's asymptotic stabilization is provided. The subsections contained herein collectively provide a comprehensive framework for the control of single-phase PWM-CSC systems.

3.1. Desired operating point

The PWM technique relies on the comparison between a reference signal operating at 10 kHz and a triangular carrier wave to generate the required switching signals. At any given instant, only two switches are active, facilitating the precise modulation of the output current. The reference waveform for the desired output voltage is defined as $x_2^\star(t) = V_p \sin(\omega t + \theta)$, where V_p represents the peak voltage, ω the angular frequency, and θ the phase angle [26].

Nonlinear control design for PWM-CSCs involves determining feasible trajectories for all the state variables. The desired operating point $(x_1^\star, x_2^\star)$ is identified by evaluating the dynamical model, which yields the following state-space equations for the desired trajectory:

$$L_i \dot{x}_1^\star = V_i - r_i x_1^\star - u^\star x_2^\star, \tag{7}$$
$$C_o \dot{x}_2^\star = u^\star x_1^\star - G_L x_2^\star. \tag{8}$$

The corresponding dynamics, derived from Equation (6), are captured by the following expression:

$$\mathcal{D}\dot{x}^\star = \left(\mathcal{J}\left(u^\star\right) - \mathcal{R}\right) x^\star + \vartheta, \tag{9}$$

where $\dot{x}^\star$ denotes the time derivative of the desired trajectory, which is nonzero in single-phase converter applications. In addition, the term $u^\star$ represents a smooth control input that is critical for maintaining the system's desired behavior. To compute $u^\star$ at the equilibrium point, Equation (7) can be utilized. However, since this approach introduces a division by $x_2^\star(t)$, a more robust method involves using Equation (8) to directly obtain the control input [6].

$$u^\star = \frac{1}{x_1^\star}\left(C_o \dot{x}_2^\star + G_L x_2^\star\right). \tag{10}$$

3.2. IDA-PBC design

Controller design using the IDA-PBC methodology is a nonlinear technique that leverages the properties of Hamiltonian systems and passivity theory [1]. This approach aims to define closed-loop dynamics to ensure stability while preserving the inherent pH structure of the system. In this vein, the primary objective of IDA-PBC is to restructure the system into a desired pH form:

$$\mathcal{D}\dot{\tilde{x}} = \mathcal{J}_d\left(u\right) - \mathcal{R}_d \tilde{x}, \tag{11}$$

where $\mathcal{J}_d(u)$ and $\mathcal{R}_d$ are the desired interconnection and dissipation matrices, respectively. These matrices are selected such that $\mathcal{R}_d$ is positive-definite and $\mathcal{J}_d(u)$ remains skew-symmetric, satisfying the condition $\mathcal{J}(u) + \mathcal{J}^\top(u) = 0$. These matrices are designed to suppress undesirable open-loop interconnections and inject sufficient damping to stabilize the system [14].

To derive the incremental model representing the system's error dynamics, the state variable errors are defined as $\tilde{x} = x - x^\star$ and $\tilde{u} = u - u^\star$. By subtracting the desired Dynamical System (9) from the Open-Loop Dynamics

(6) and performing some algebraic manipulations, the incremental error model is obtained, as shown in Equation (12).

$$\mathcal{D}\dot{\tilde{x}} = \mathcal{J}\left(\tilde{u}\right)x^{\star} + \left(\mathcal{J}\left(u\right) - \mathcal{R}\right)\tilde{x}, \tag{12}$$

To design the closed-loop controller, the Open-Loop Dynamics (11) are equated with the Desired Dynamics (12), resulting in Equation (13).

$$\mathcal{J}\left(\tilde{u}\right)x^{\star} + \left(\mathcal{J}\left(u\right) - \mathcal{R}\right)\tilde{x} = \left(\mathcal{J}_d - \mathcal{R}_d\right)\tilde{x}, \tag{13}$$

$$\mathcal{J}\left(\tilde{u}\right)x^{\star} = \mathcal{J}_1 - \left(\mathcal{R}_d - \mathcal{R}\right)\tilde{x}, \tag{14}$$

The solution to Equation (14) depends on the appropriate selection of the desired interconnection matrix, dissipation matrix, and Hamiltonian function. This selection is as follows:

$$\mathcal{J}_d = \mathcal{J}\left(u\right) + \mathcal{J}_1$$

where:

$$\mathcal{J}_d = \begin{pmatrix} 0 & -\omega \\ \omega & 0 \end{pmatrix}, \mathcal{R}_d = \begin{pmatrix} R_1 & 0 \\ 0 & R_2 \end{pmatrix}, \tag{15}$$

The resulting control law is obtained by solving Equation (14), which yields

$$\tilde{u} = \left(g\left(x^{\star}\right)^{\top} g\left(x^{\star}\right)\right)^{-1} g\left(x^{\star}\right)^{\top}\left(\mathcal{J}_1 - \left(\mathcal{R}_d - \mathcal{R}\right)\tilde{x}\right), \tag{16}$$

where

$$g\left(x^{\star}\right) = \begin{pmatrix} -x_2^{\star} \\ x_1^{\star} \end{pmatrix}.$$

The complete control input, incorporating the incremental and equilibrium components, is expressed as follows:

$$\tilde{u} = \frac{1}{x_1^{\star} + x_2^{\star}}\begin{pmatrix} -x_2^{\star} & x_1^{\star} \end{pmatrix}\left[\begin{pmatrix} 0 & -\omega \\ \omega & 0 \end{pmatrix} - \left(\begin{pmatrix} R_1 & 0 \\ 0 & R_2 \end{pmatrix} - \begin{pmatrix} r_i & 0 \\ 0 & G_L \end{pmatrix}\right)\right]\begin{pmatrix} -\tilde{x}_2 \\ \tilde{x}_1 \end{pmatrix} \tag{17}$$

By substituting the expressions with $u = u^{\star} + \tilde{u}$, the full control input in Equation (18) is obtained.

$$u = \frac{1}{x_1^{\star}}\left(C_o\dot{x}_2^{\star} + G_L x_2^{\star}\right) + \frac{1}{x_1^{*} + x_2^{*}}\begin{pmatrix} -x_2^{*} & x_1^{*} \end{pmatrix}\left[\begin{pmatrix} 0 & -\omega \\ \omega & 0 \end{pmatrix} - \left(\begin{pmatrix} R_1 & 0 \\ 0 & R_2 \end{pmatrix} - \begin{pmatrix} r_i & 0 \\ 0 & G_L \end{pmatrix}\right)\right]\begin{pmatrix} -\tilde{x}_2 \\ \tilde{x}_1 \end{pmatrix} \tag{18}$$

To verify the closed-loop asymptotic stability of the proposed controller, consider the Lyapunov function $\mathcal{V}\left(\tilde{x}\right) = \frac{1}{2}\tilde{x}^{\top}\mathcal{D}\tilde{x}$, which satisfies $\mathcal{V} > 0$ and $\mathcal{V}(0) = 0$ [19]. The time derivative of $\mathcal{V} > 0$ is computed as follows:

$$\begin{aligned} \dot{\mathcal{V}}\left(\tilde{x}\right) &= \tilde{x}^{\top}\mathcal{D}\dot{\tilde{x}}, \\ &= \tilde{x}^{\top}\left(\left(\mathcal{J}\left(u\right) + \mathcal{J}_1\right) - \mathcal{R}_d\right)\dot{\tilde{x}}, \\ &= -\tilde{x}^{\top}\mathcal{R}_d\tilde{x} < 0. \end{aligned} \tag{19}$$

This confirms the asymptotic stability of the closed-loop system in the sense of Lyapunov, ensuring that $x \to x^{\star}$ as $t \to \infty$ [15].

3.3. PI-PBC design

PI-PBC combines the benefits of passivity-based design with proportional and integral components, thereby enhancing state regulation, disturbance rejection, and reference tracking performance [7]. This methodology is especially effective for dynamical systems represented by pH models, as it exploits their inherent energy structure to ensure stability in the sense of Lyapunov [22].

This subsection provides a detailed formulation of the PI-PBC, including its mathematical derivation, stability analysis, and performance evaluation.

The incremental model described in Equation (12) can be asymptotically stabilized by defining a suitable PI control law [12]. This control law drives the system to a stable equilibrium at $\tilde{x} = 0$ when the control input $\tilde{u} = 0$ is defined as follows:

$$\begin{aligned} \tilde{u} &= -k_p \tilde{y} - k_i \tilde{z}, \\ \dot{\tilde{z}} &= \tilde{y}, \end{aligned} \tag{20}$$

where k_p and k_i are positive control gains, and $\tilde{y}$ denotes the passive output of the system. The passive output $\tilde{y}$ is computed as shown below.

$$\tilde{y} = x^{\star,\top} \mathcal{J}_1 \tilde{x} = \begin{bmatrix} x_1^\star & x_2^\star \end{bmatrix} \begin{bmatrix} 0 & -1 \\ 1 & 0 \end{bmatrix}^\top \begin{bmatrix} \tilde{x}_1 \\ \tilde{x}_2 \end{bmatrix} \implies \tilde{y} = x_1^\star \tilde{x}_2 - x_2^\star \tilde{x}_1. \tag{21}$$

This yields the following PI-PBC control law:

$$\tilde{u} = -k_p \left(x_1^\star \tilde{x}_2 - x_2^\star \tilde{x}_1 \right) - k_i \int_0^{t_f} \left(x_1^\star \tilde{x}_2 - x_2^\star \tilde{x}_1 \right) d\tau. \tag{22}$$

Considering that $u = u^\star + \tilde{u}$, and incorporating the expressions from Equations (8) and (22), the control input is expressed as

$$u = \frac{1}{x_1^\star} \left(C_o \dot{x}_2^\star + G_L x_2^\star \right) - k_p \left(x_1^\star \tilde{x}_2 - x_2^\star \tilde{x}_1 \right) - k_i \int_0^{t_f} \left(x_1^\star \tilde{x}_2 - x_2^\star \tilde{x}_1 \right) d\tau. \tag{23}$$

To verify the asymptotic stability of the proposed controller in closed-loop operation, the following candidate Lyapunov function is considered: $\mathcal{V}(\tilde{x}, \tilde{z}) = \frac{1}{2} \tilde{x}^\top \mathcal{D} \tilde{x} + \frac{1}{2} k_i \tilde{z}^2$, which is positive definite and satisfies $\mathcal{V}(0) = 0$ [24]. By differentiating this function with respect to time, the following is obtained:

$$\begin{aligned} \dot{\mathcal{V}}(\tilde{x}, \tilde{z}) &= \tilde{x}^\top \mathcal{D} \dot{\tilde{x}} + k_i \tilde{z} \dot{\tilde{z}}, \\ &= \tilde{x}^\top \left(\mathcal{J}(\tilde{u}) x^\star + \left(\mathcal{J}(u) - \mathcal{R} \right) \tilde{x} \right) + k_i \tilde{z} \tilde{y} \\ &= -\tilde{x}^\top \mathcal{R} \tilde{x} - \tilde{y}^\top k_p \tilde{y} < 0, \end{aligned} \tag{24}$$

indicating that the dynamical system described by Equation (14) is asymptotically stable in the sense of Lyapunov, *i.e.*, $x \to x^\star$ as $t \to \infty$.

3.4. Nonlinear PI control design

The proposed nonlinear PI controller aims to guarantee the asymptotic convergence of x_2 while ensuring a tightly regulated behavior of x_1 for all $t \geq 0$ [10]. To this effect, it is assumed that the function tracking the reference is expressed as

$$x_1 = I_s + I_h \sin(2\omega t + \varphi), \tag{25}$$

where I_s represents the DC component of x_1, and the frequency is twice that of the AC side. The amplitude of the harmonic ripple, denoted as I_h, is determined by

$$I_h = \sqrt{\left(\frac{V_i^2}{4\omega L_i I_s R_L}\right)^2 + \left(\frac{CV_i^2}{4L_i I_s}\right)^2}, \tag{26}$$

while the phase is given by

$$\varphi = \tan^{-1}(\omega C_o R_L). \tag{27}$$

The control input for the nonlinear PI controller is formulated as follows:

$$\tilde{u} = -k_p \tilde{x}_2 - k_i \int_0^t \tilde{x}_2, \tag{28}$$

where k_p and k_i are positive constants that define the proportional and integral actions, respectively. Here, $\tilde{x}_2 = x_2 - x_2^*$ represents the error term, which is designed to converge to zero.

Considering that the total control input is $u = u^* + \tilde{u}$, and by substituting the expressions in Equations (8) and (28) [12], the control input can be rewritten as follows:

$$u = \frac{1}{x_1^*}\left(C_o \dot{x}_2^* + G_L x_2^*(t) - k_p \tilde{x}_2 - k_i \int_0^t \tilde{x}_2\right), \tag{29}$$

To analyze the stability of the system under the proposed control law, the Lyapunov stability theorem is employed. This theorem states that the existence of a positive-definite Lyapunov function $\mathcal{V}(x)$ whose time derivative $\dot{\mathcal{V}}(x)$ is negative-definite ensures the global asymptotic stability of the equilibrium point. For the proposed controller, this implies that the equilibrium states (x_1, x_2) converge to their desired values as $t \to \infty$, thereby achieving global asymptotic stability [16].

4. Simulations and results

The proposed controller design was implemented in a simulated environment using the MATLAB software, version 2023b. For the simulation, the following parameter values were defined to interpret the results: $V_p = 150V$, $V_i = 48V$, $L_i = 10mH$, $C_o = 200\mu F$, and $r_i = 1\Omega$. These values were selected according to the work by [8]. The numerical integration was performed using the backward Euler method, with a fixed sampling period of $1\mu s$, ensuring an adequate resolution for accurately capturing the switching dynamics inherent to PWM-based control.

To facilitate the practical implementation of the proposed control strategies, certain simplifications and methodological guidelines were adopted. For instance, all controllers were designed while assuming full state measurement availability, which, though ideal, can be approximated in real applications through observer-based estimation techniques.

The IDA-PBC was implemented $R_1 = 150$ and $R_2 = 10.000$. This configuration ensures excellent tracking of both current and voltage references, as depicted in Figure 2. The THD obtained was remarkably low, at 0.0986%, demonstrating the method's effectiveness in maintaining signal fidelity.

The PI-PBC was implemented with $k_p = 1.5$ and $k_i = 0.8$. This tuning allows for the precise tracking of current and voltage references, as illustrated in Figure 3. The resulting THD was 0.096%, slightly outperforming IDA-PBC in terms of harmonic distortion reduction while maintaining a robust performance.

The nonlinear PI controller was implemented with $k_p = 0.1$ and $k_i = 0.4$. This configuration provides adequate tracking of current and voltage references, as observed in Figure 4. However, the reported THD was 2.52%, which, while acceptable, is significantly higher than the values obtained by IDA-PBC and PI-PBC.

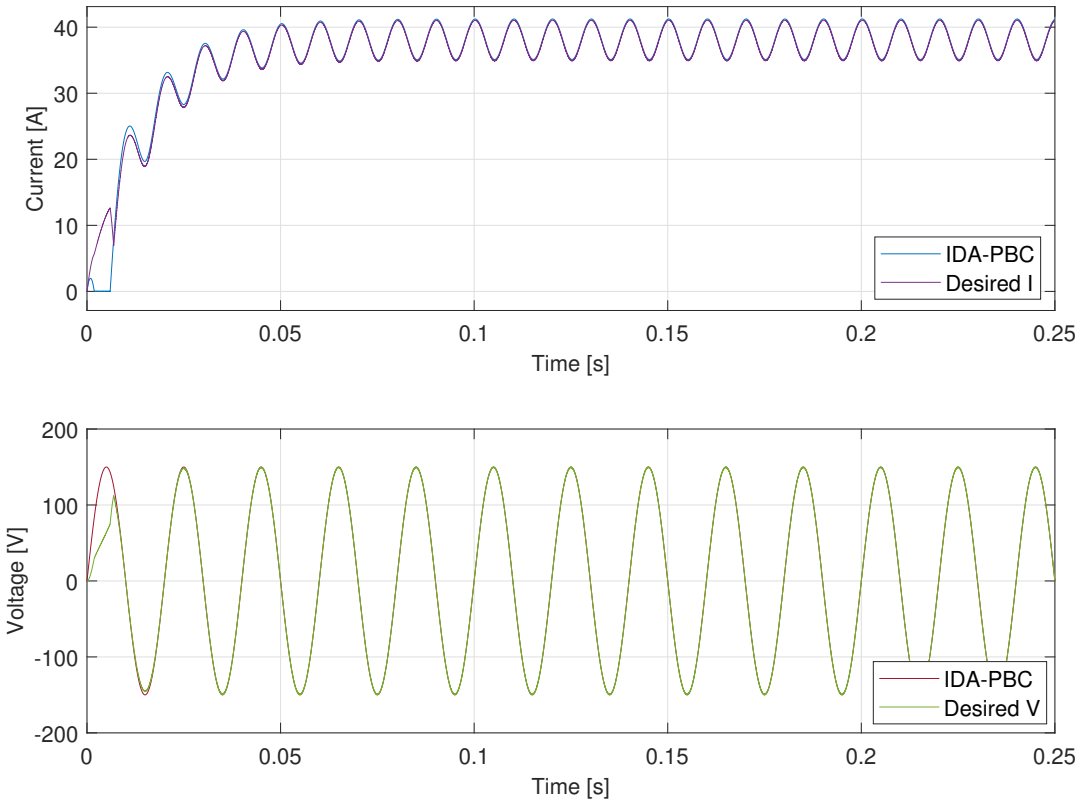

Figure 2. Voltage and current tracking performance with IDA-PBC

Among the three control strategies, IDA-PBC and PI-PBC demonstrated superior performance in terms of tracking accuracy and harmonic distortion minimization, achieving THD values of 0.0986% and 0.096%, respectively. While the nonlinear PI controller provided acceptable reference tracking, its THD of 2.52% indicates a lower capacity for harmonic distortion mitigation when compared to the passivity-based approaches. Overall, PI-PBC emerges as the most effective strategy, offering both robust tracking and the lowest harmonic distortion.

Table 1. Control parameter comparison

Parameter	**Desired**	**IDA-PBC**	**PI-PBC**	**Nonlinear PI**
V_p	150 V	150 V	149.3 V	149.7 V
V_{rms}	106.06 V	106.1 V	105.6 V	105.8 V
THD_v	0%	0.0986%	0.096%	2.519%
I_p	3 A	3 A	2.986 A	2.993 A
I_{rms}	2.121 A	2.121 A	2.112 A	2.117 A
THD_I	0%	0.0986%	0.096%	2.519%
Steady-state error $\max_I$	0	0.028 A	0.019 A	0.011 A
Steady-state error $\max_v$	0	1 mV	5 mV	40 mV
Settling Time	7 ms	6 ms	9 ms	25 ms

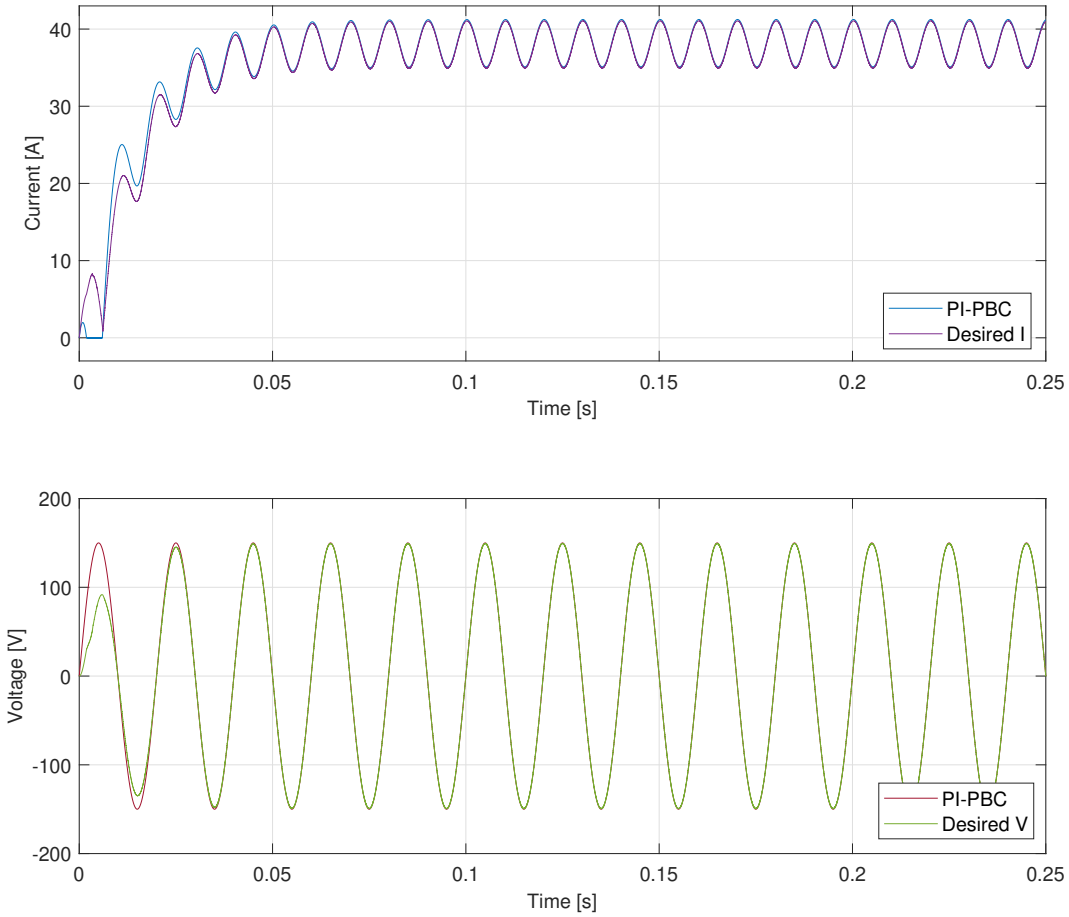

Figure 3. Voltage and current tracking performance with PI-PBC

Figures 5 and 6 compare the performance of the three control strategies, which were simultaneously evaluated in terms of voltage and current tracking, harmonic distortion, steady-state error, and settling time. All controllers reported values close to the desired peak voltage of 150 V. IDA-PBC performed exactly at the desired value, while PI-PBC and nonlinear PI control slightly undershot, with 149.3 V and 149.7 V, respectively.

IDA-PBC delivered the closest match (106.1 V) to the desired root mean square (RMS) voltage of 106.06 V. PI-PBC obtained 105.6 V, and the nonlinear PI controller performed similarly, with 105.8 V. Both IDA-PBC and PI-PBC maintained a very low harmonic distortion, with THD_v values of 0.0986% and 0.096%, respectively. However, nonlinear PI control exhibited a significantly higher THD_v of 2.519%, indicating poorer harmonic suppression.

IDA-PBC reached the desired current peak of 3 A, whereas PI-PBC and nonlinear PI control slightly underperformed, with 2.986 A and 2.993 A, respectively. All controllers closely followed the desired RMS current of 2.121 A. IDA-PBC reached the exact value, while PI-PBC and nonlinear PI control showed slight deviations, with 2.112 A and 2.117 A.

Nonlinear PI control reported the lowest maximum error (0.011 A), followed by PI-PBC with 0.019 A and IDA-PBC with 0.028 A. IDA-PBC achieved the lowest voltage error (1 mV), while PI-PBC and nonlinear PI control

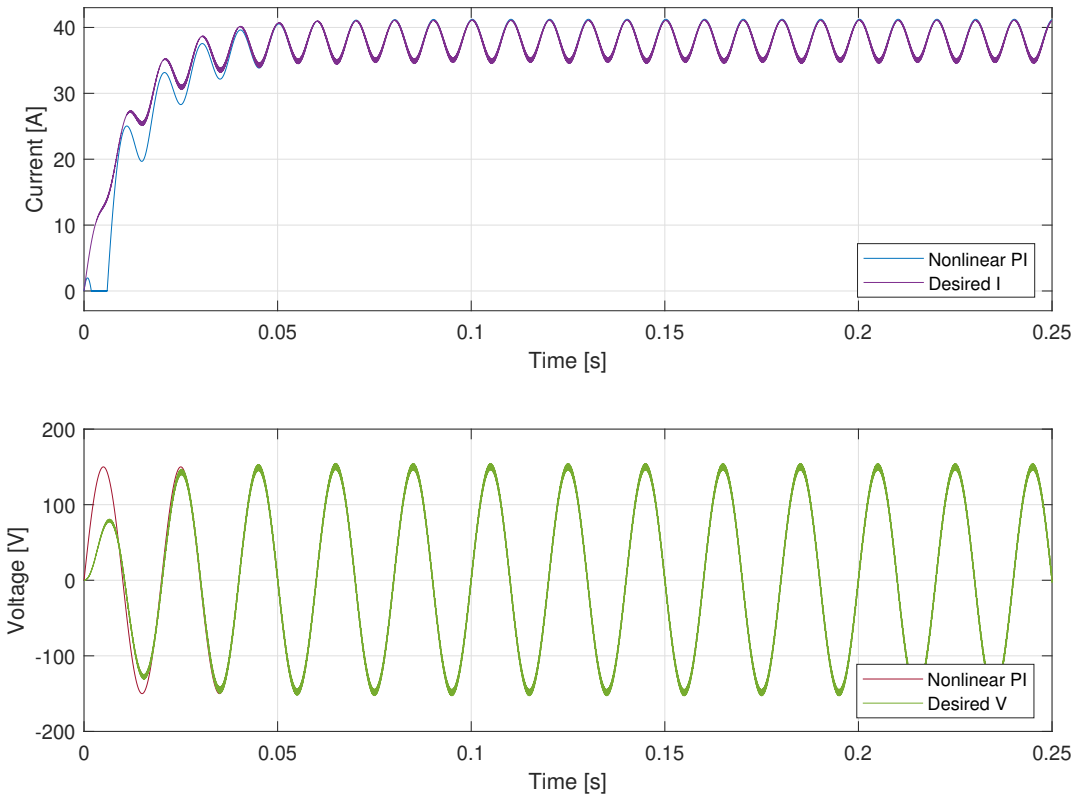

Figure 4. Voltage and current tracking performance with nonlinear PI control

exhibited values of 5 mV and 40 mV, respectively. IDA-PBC demonstrated the fastest settling time (6 ms), followed by PI-PBC (9 ms). Nonlinear PI control showed a significantly slower response, with a settling time of 25 ms.

Overall, IDA-PBC and PI-PBC indicated a comparable and superior performance in terms of harmonic suppression, steady-state accuracy, and response time. While nonlinear PI control achieved acceptable current and voltage tracking, it fell short in terms of harmonic distortion mitigation and settling time, making it less effective under these operating conditions. Table 1 provides a comprehensive quantitative comparison of the parameters that support these conclusions.

In order to evaluate the high-frequency performance of the proposed control strategies and analyze potential trade-offs associated with electromagnetic interference (EMI), simulations were conducted at three different commutation frequencies: 10 kHz, 50 kHz, and 100 kHz. The THD was measured in terms of both current and voltage. A record was kept for each case, as presented in Table 2.

According to our findings, the passivity-based controllers (IDA-PBC and PI-PBC) exhibit a substantial degree of resilience to increments in the switching frequency. Specifically, the THD for the IDA-PBC controller increases marginally from 0.0986% at 10 kHz to 0.1103% at 100 kHz. In a similar way, PI-PBC exhibits minimal distortion across the entire frequency spectrum, exhibiting a slight increase from 0.096% to 0.1056%. This suggests that both controllers maintain their harmonic performance even under high-frequency switching conditions, a desirable characteristic in applications where reduced filter size and improved dynamic response are required.

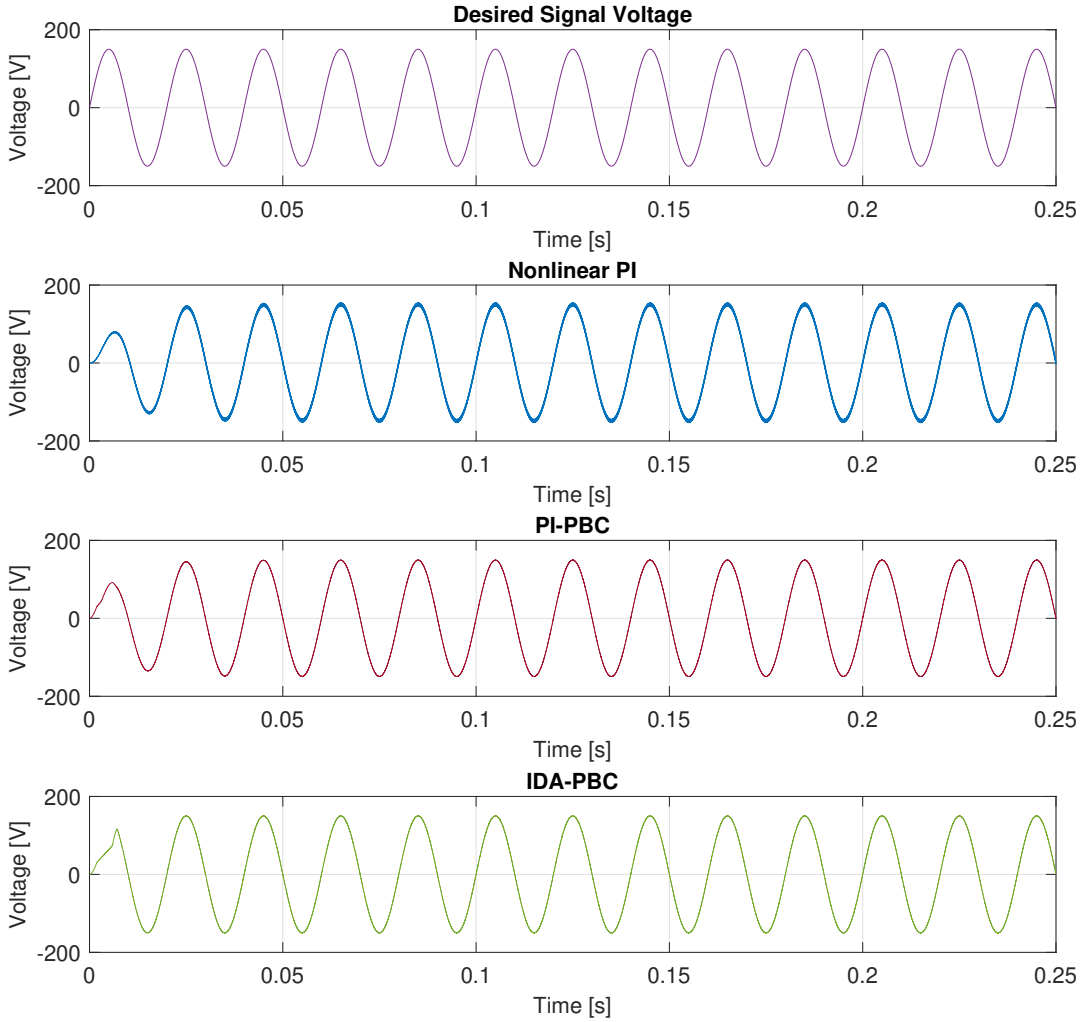

Figure 5. Voltage tracking performance comparison

Conversely, the nonlinear PI controller demonstrates a marked degradation in THD as the switching frequency rises. The initial THD of 2.519% at 10 kHz rises to 6.532% at 50 kHz and reaches 14.1% at 100 kHz. This trend suggests a heightened sensitivity to high-frequency effects, likely attributable to the absence of internal energy-balancing mechanisms and increased vulnerability to high-frequency switching noise and EMI.

These results underscore a salient trade-off: while increasing the switching frequency can enhance the control resolution and reduce the size of passive components, it may concomitantly exacerbate EMI and harmonic issues, particularly in controllers with no structural energy-conserving properties. Consequently, in high-frequency applications (*e.g.*, power converters for electric vehicle chargers or grid-tied inverters), passivity-based strategies such as IDA-PBC and PI-PBC offer a more favorable compromise between performance, stability, and EMI robustness.

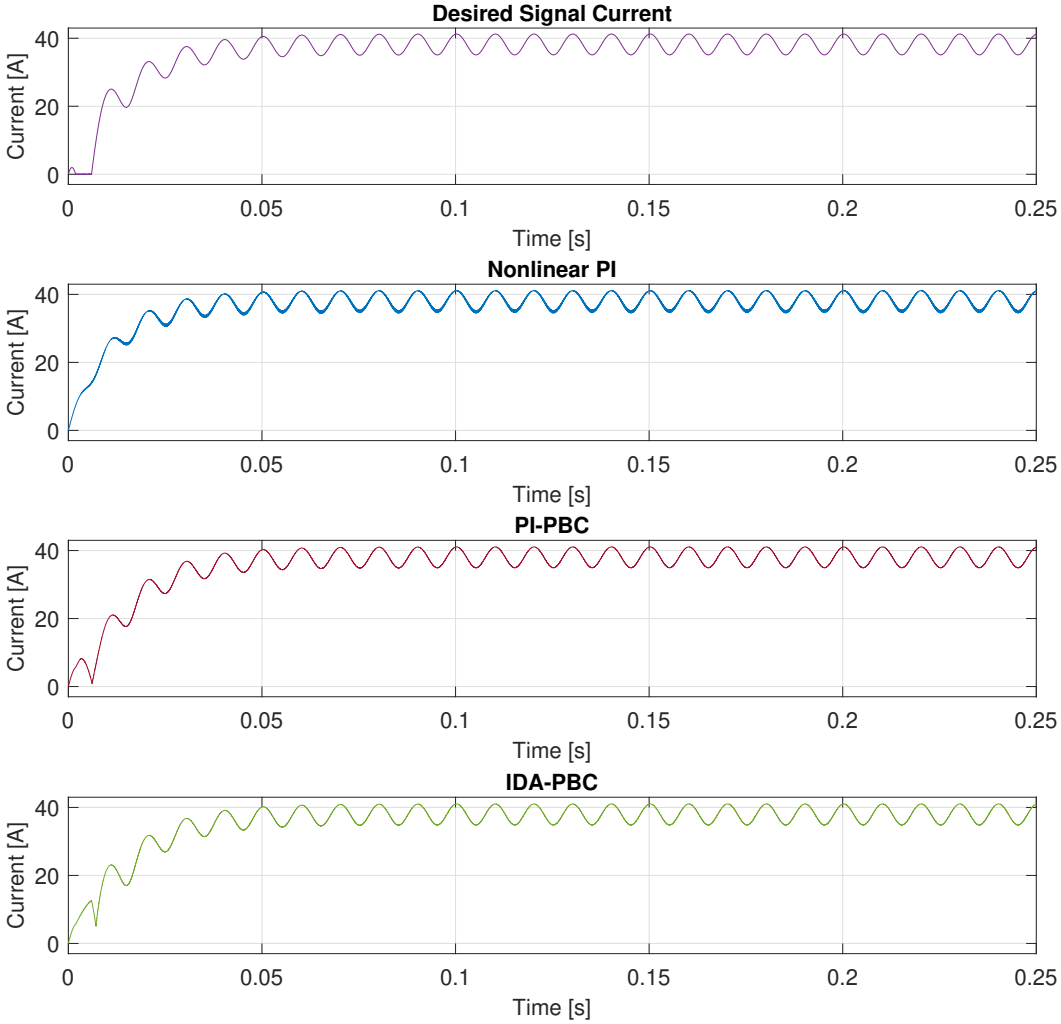

Figure 6. Current tracking performance comparison

4.1. Discussion of trade-offs

A comparative analysis is presented in Table 3. This evaluation provides a summary of the strengths and limitations of each control strategy, *i.e.*, IDA-PBC, PI-PBC, and nonlinear PI, highlighting their practical implications for real-time implementation in power converter applications.

While IDA-PBC has been shown to achieve excellent signal fidelity and the fastest transient response, its implementation is complex due to the necessity of nonlinear modeling, pH formalism, and matrix manipulation. PI-PBC offers a balanced compromise, achieving a marginally better THD than IDA-PBC while maintaining acceptable transient behavior with moderate complexity, which is attributed to the scalar gain structure integrated into the passivity-based framework. Conversely, the nonlinear PI controller, despite its simplicity in implementation, exhibits suboptimal performance in terms of harmonic suppression and settling time, consequently

Table 2. THD performance at high commutation frequencies for each control strategy

Control strategy	Commutation frequency	$\text{THD}_i/\text{THD}_v$
IDA-PBC	10 kHz	0.0986%
	50 kHz	0.1037%
	100 kHz	0.1103%
PI-PBC	10 kHz	0.096%
	50 kHz	0.1002%
	100 kHz	0.1056%
Nonlinear PI	10 kHz	2.519%
	50 kHz	6.532%
	100 kHz	14.1%

Table 3. Summary of control strategies for converters

Control strategy	THD (%)	Settling time (ms)	Implementation complexity	Remarks
IDA-PBC	0.0986	6	High	Excellent tracking and stability with minimal THD. Requires Hamiltonian modeling and matrix synthesis.
PI-PBC	0.096	9	Moderate	Slightly better THD than IDA-PBC; simpler structure due to scalar gains – still, it preserves passivity.
Nonlinear PI	2.519	25	Low	Simplest to implement but shows significant degradation in THD and a slower transient behavior.

limiting its suitability for applications that require high power quality. Consequently, PI-PBC is identified as the most practical solution for scenarios that require low harmonic distortion and moderate implementation effort.

A sensitivity analysis was performed by introducing $\pm 20\%$ variations in key system parameters: the load resistance (R_L), the input inductance (L_i), and the output capacitance C_o. The resulting current responses for each controller are illustrated in Figure 7. The responses reveal that both IDA-PBC and PI-PBC maintain high tracking performance and exhibit minimal deviations under parameter perturbations. In contrast, the nonlinear PI controller exhibits greater sensitivity to such variations, resulting in more pronounced oscillations and transient deviations. These results highlight the superior robustness of passivity-based approaches, particularly under uncertain operating conditions, reinforcing their suitability for practical applications that require consistent performance despite parameter mismatches.

4.2. Extended discussion: adaptive enhancements and industrial comparisons

Adaptive or gain-scheduled extensions to NPI control. While the nonlinear PI controller demonstrated acceptable performance in tracking reference signals, its elevated THD (2.52%) compared to passivity-based approaches reveals some room for improvement. In this regard, incorporating adaptive control mechanisms or gain scheduling strategies could enhance the controller's ability to mitigate harmonics under varying operational conditions.

Adaptive PI controllers dynamically adjust proportional and integral gains in response to real-time variations in system states or parameters. This feature is particularly advantageous in systems subject to load uncertainty, input voltage fluctuations, or parametric drift. For instance, adopting model reference adaptive control or *extremum*-seeking techniques may allow the nonlinear PI controller to respond more effectively to nonlinearities or disturbances. In a similar way, gain-scheduled PI controllers employ pre-defined mappings from operating conditions to controller gains, improving performance across a wider range of scenarios without compromising simplicity.

Tuning effort comparison. One of the primary challenges associated with nonlinear PI control lies in the manual tuning process. As demonstrated in this study, the chosen gains $(kp = 0.1, ki = 0.4)$ required iterative adjustment to balance steady-state error and THD. This contrasts with the PI-PBC and IDA-PBC methods, where the design

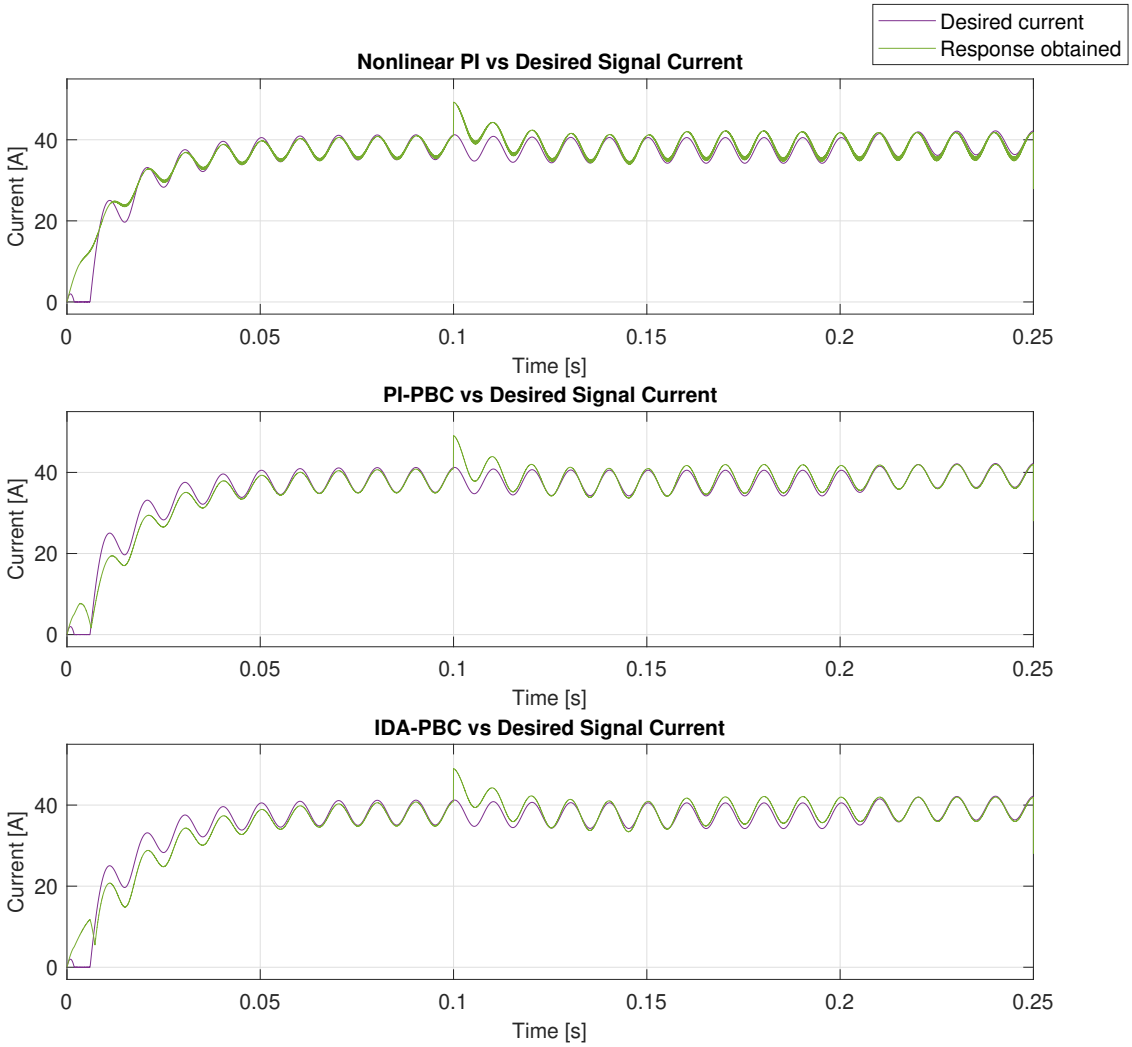

Figure 7. Current tracking performance under parameter variations

process is rooted in a formal mathematical framework (*e.g.*, Lyapunov-based stability criteria and pH structures), thereby reducing reliance on empirical tuning.

While passivity-based controllers also involve parameter selection (*e.g.*, Rd in IDA-PBC or kp, ki in PI-PBC), these are derived within a structure-preserving context, allowing for a more systematic and reproducible design. The nonlinear PI controller, in contrast, lacks intrinsic design constraints, which can lead to suboptimal or inconsistent outcomes depending on the designer's expertise.

Comparison with industry-standard controllers. In industrial applications, conventional PI and PID controllers remain the *de facto* standard due to their simplicity, intuitive tuning, and widespread implementation in digital control platforms. However, these controllers often rely on linearized system models and perform suboptimally in systems with high nonlinearities or fast dynamics, such as PWM-CSCs.

When compared to these industry-standard controllers, the nonlinear PI, PI-PBC, and IDA-PBC methods offer improved tracking accuracy, lower THD, and guaranteed stability under broader conditions. Nevertheless,

traditional PI/PID controllers still hold advantages in terms of implementation simplicity, computational efficiency, and diagnostic familiarity.

5. Conclusion

This study provides a comprehensive analysis of various control techniques applied to PWM-CSCs *i.e.*, IDA-PBC, PI-PBC, and nonlinear PI control. Based on the results obtained, the following conclusions can be drawn:

i. IDA-PBC and PI-PBC proved to be highly effective in tracking current and voltage references, achieving low THD levels of 0.0986% and 0.096%, respectively. This highlights their ability to maintain signal integrity compared to nonlinear PI control, which reported a significantly higher THD (2.52%).
ii. The application of Lyapunov stability theory in designing the controllers ensured the global asymptotic stability of the system's equilibrium points. This provides a solid foundation for the practical implementation of these techniques, ensuring that the system states converge to their desired values over time.
iii. The results have significant implications for the implementation of controllers in renewable energy systems and other industrial applications where precise current control and harmonic distortion minimization are critical to system performance.

Future directions. Based on the findings of this study, several promising avenues can be proposed for further research into the control of PWM-CSCs. Firstly, extending the analysis to systems that feed non-linear loads, such as constant power loads (CPLs), diode bridge rectifiers, or non-linear impedances, would allow evaluating the proposed control strategies under more realistic and challenging conditions. Such scenarios often exacerbate stability and harmonic issues, thus providing a more stringent benchmark for controller performance.

Secondly, the proposed single-phase control strategies could be scaled up to three-phase configurations, which are prevalent in industrial applications and grid-connected systems. The pH framework and passivity-based methodologies provide a structured basis for generalizing the control laws for multi-phase systems while preserving their energy-based interpretability and stability guarantees.

Furthermore, a comparative assessment of the computational demands associated with each control method (PI-PBC, IDA-PBC, nonlinear PI) would offer valuable insights for hardware implementation. Such analysis is imperative for embedded applications, where processor capabilities and execution times are constrained. In a similar vein, the robustness of the controllers against sensor noise and their immunity to measurement disturbances should be systematically evaluated, potentially incorporating noise-rejection filters or redesigning the control law to enhance resilience.

Future research should also concentrate on the design of state observers or estimators, particularly in scenarios where full state measurement is not viable. The integration of sliding-mode observers, extended Kalman filters, or adaptive estimation techniques could facilitate the reconstruction of unmeasured states with sufficient accuracy and robustness.

In addition, it would be beneficial to perform a comparative analysis of the proposed strategies against advanced control techniques such as finite control set model predictive control (FCS-MPC) or adaptive backstepping. These methods offer high-performance capabilities but typically incur greater computational costs or model complexity. This analysis would highlight the trade-offs in accuracy, robustness, and implementation feasibility.

It is imperative to recognize the significance of experimental validation as a pivotal component in the transition towards real-world deployment. It is recommended that future studies incorporate hardware-in-the-loop (HIL) simulations with a view to validating the effectiveness of the controllers under real-time constraints. Furthermore, the identification of discrepancies between simulated and experimental results, including but not limited to parasitic elements, delays, quantization effects, or model mismatches, would facilitate the refinement of control design and enhance practical reliability.

Emerging research could also explore the integration of artificial intelligence (AI) techniques, including reinforcement learning or neural-network-enhanced control, to automate tuning processes or adapt to highly dynamic environments. These approaches have the potential to complement traditional control strategies, especially in contexts where accurate modeling is impractical or system parameters undergo rapid changes.

Finally, the control strategies developed in this work are well suited for emerging domains such as electric vehicle charging systems, renewable energy inverters, or smart grid interfaces. Adapting the proposed methods to such applications could facilitate a robust and efficient power conversion, thereby addressing pressing challenges in modern energy systems.

ACKNOWLEDGEMENTS

The first author would like to express gratitude to the Doctoral Program in Engineering at Universidad Distrital Francisco José de Caldas for its invaluable support during this research. The academic and institutional resources provided were essential to the successful completion of this study.

REFERENCES

1. Beckers, T.: Data-Driven Bayesian Control of Port-Hamiltonian Systems. In: 2023 62nd IEEE Conference on Decision and Control (CDC). IEEE (Dec 2023). https://doi.org/10.1109/cdc49753.2023.10384219
2. Buccella, C., Cecati, C., Latafat, H.: Digital Control of Power Converters—A Survey. IEEE Transactions on Industrial Informatics **8**(3), 437–447 (Aug 2012). https://doi.org/10.1109/tii.2012.2192280
3. Gil-Gonzalez, W., Montoya, O.D., Garces, A., Espinosa-Perez, G.: IDA-Passivity-Based Control for Superconducting Magnetic Energy Storage with PWM-CSC pp. 89–95 (Mar 2017). https://doi.org/10.1109/greentech.2017.19
4. Gil-González, W., Montoya, O.D., Riffo, S., Restrepo, C., Muñoz, J.: A global tracking sensorless adaptive pi-pbc design for output voltage regulation in a boost converter feeding a dc microgrid. Energies **16**(3), 1106 (Jan 2023). https://doi.org/10.3390/en16031106
5. Gómez-Estern, F., Van der Schaft, A.: Physical Damping in IDA-PBC Controlled Underactuated Mechanical Systems. European Journal of Control **10**(5), 451–468 (Jan 2004). https://doi.org/10.3166/ejc.10.451-468
6. Hava, A.M., Kerkman, R.J., Lipo, T.A.: Carrier-based pwm-vsi overmodulation strategies: Analysis, comparison, and design. IEEE Transactions on Power Electronics **13**, 674–689 (1998). https://doi.org/10.1109/63.704136
7. He, W., Namazi, M.M., Koofigar, H.R., Amirian, M.A., Blaabjerg, F.: Stabilization of dc–dc buck converter with unknown constant power load via passivity-based control plus proportion-integration. IET Power Electronics **14**(16), 2597–2609 (Nov 2021). https://doi.org/10.1049/pel2.12205
8. Komurcugil, H.: Nonlinear control strategy for single-phase pwm current-source inverters. In: 2009 35th Annual Conference of IEEE Industrial Electronics. IEEE (Nov 2009). https://doi.org/10.1109/iecon.2009.5415002
9. Kwasinski, A., Onwuchekwa, C.N.: Dynamic Behavior and Stabilization of DC Microgrids With Instantaneous Constant-Power Loads. IEEE Transactions on Power Electronics **26**(3), 822–834 (Mar 2011). https://doi.org/10.1109/tpel.2010.2091285
10. Liu, P., Wang, Z., Wei, S., Bo, Y., Pu, S.: Recent developments of modulation and control for high-power current-source-converters fed electric machine systems. CES Transactions on Electrical Machines and Systems **4**(3), 215–226 (Sep 2020). https://doi.org/10.30941/cestems.2020.00027
11. Mandrile, F., Musumeci, S., Carpaneto, E., Bojoi, R., Dragičević, T., Blaabjerg, F.: State-Space Modeling Techniques of Emerging Grid-Connected Converters. Energies **13**(18), 4824 (Sep 2020). https://doi.org/10.3390/en13184824
12. Montoya, O.D., Acevedo, O., Gil-González, W., Holguín, M., Serra, F.M.: On the nonlinear control of a single-phase current source converter for sinusoidal voltage generation. Journal of Physics: Conference Series **1448**(1), 012011 (Jan 2020). https://doi.org/10.1088/1742-6596/1448/1/012011
13. Montoya, O., Gil-Gonzalez, W., Garces, A., Serra, F., Hernandez, J.: Pi-pbc approach for voltage regulation in Ćuk converters with adaptive load estimation. In: 2020 IEEE International Autumn Meeting on Power, Electronics and Computing (ROPEC). IEEE (Nov 2020). https://doi.org/10.1109/ropec50909.2020.9258716
14. Montoya, O.D., Gil-González, W., Garces, A.: Distributed energy resources integration in single-phase microgrids: An application of ida-pbc and pi-pbc approaches. International Journal of Electrical Power & Energy Systems **112**, 221–231 (Nov 2019). https://doi.org/10.1016/j.ijepes.2019.04.046
15. Montoya, O.D., Gil-González, W., Garcés, A., Espinosa-Pérez, G.: Indirect ida-pbc for active and reactive power support in distribution networks using smes systems with pwm-csc. Journal of Energy Storage **17**, 261–271 (6 2018). https://doi.org/10.1016/J.EST.2018.03.004
16. Ortega, R., Astolfi, A., Barabanov, N.E.: Nonlinear pi control of uncertain systems: an alternative to parameter adaptation. Systems & Control Letters **47**(3), 259–278 (Oct 2002). https://doi.org/10.1016/s0167-6911(02)00212-8
17. Ortega, R., Donaire, A., Romero, J.G.: Passivity-Based Control of Mechanical Systems, pp. 167–199. Springer International Publishing (2017). https://doi.org/10.1007/978-3-319-51298-3_7
18. Pang, S., Nahid-Mobarakeh, B., Hashjin, S.A., Pierfederici, S., Martin, J.P., Liu, Y., Huangfu, Y., Luo, G., Gao, F.: Stability Improvement of Cascaded Power Conversion Systems Based on Hamiltonian Energy Control Theory. IEEE Transactions on Industry Applications **57**(1), 1081–1093 (Jan 2021). https://doi.org/10.1109/tia.2020.3038355
19. Ramírez, H., Sbarbaro, D., Ortega, R.: On the control of non-linear processes: An ida–pbc approach. Journal of Process Control **19**, 405–414 (3 2009). https://doi.org/10.1016/J.JPROCONT.2008.06.018
20. Rosa, A., Morais, L., Fortes, G., Seleme Júnior, S.: Practical considerations of nonlinear control techniques applied to static power converters: A survey and comparative study. International Journal of Electrical Power & Energy Systems **127**, 106545 (May 2021). https://doi.org/10.1016/j.ijepes.2020.106545

21. Sanders, S., Verghese, G.: Lyapunov-based control for switched power converters. IEEE Transactions on Power Electronics **7**(1), 17–24 (Jan 1992). https://doi.org/10.1109/63.124573
22. Schaft, A.J.V.D.: Port-hamiltonian systems: Network modeling and control of nonlinear physical systems. Advanced Dynamics and Control of Structures and Machines pp. 127–167 (2004). https://doi.org/10.1007/978-3-7091-2774-2-9
23. van der Schaft, A., Maschke, B.: Dirac and lagrange algebraic constraints in nonlinear port-hamiltonian systems. Vietnam Journal of Mathematics **48**(4), 929–939 (Jun 2020). https://doi.org/10.1007/s10013-020-00419-x
24. Serra, F.M., Fernández, L.M., Montoya, O.D., Gil-González, W., Hernández, J.C.: Nonlinear Voltage Control for Three-Phase DC-AC Converters in Hybrid Systems: An Application of the PI-PBC Method. Electronics **9**(5), 847 (May 2020). https://doi.org/10.3390/electronics9050847
25. Tahir, S., Wang, J., Baloch, M., Kaloi, G.: Digital control techniques based on voltage source inverters in renewable energy applications: A review. Electronics **7**(2), 18 (Feb 2018). https://doi.org/10.3390/electronics7020018
26. Trzynadlowski, A.M.: Overview of modern pwm techniques for three-phase, voltage-controlled, voltage-source inverters. IEEE International Symposium on Industrial Electronics **1**, 25–39 (1996). https://doi.org/10.1109/ISIE.1996.548389
27. Tõnso, M., Kaparin, V., Belikov, J.: Port-Hamiltonian framework in power systems domain: A survey. Energy Reports **10**, 2918–2930 (Nov 2023). https://doi.org/10.1016/j.egyr.2023.09.077
28. Zhang, Y., Li, Y.: Current Source Converters and Their Control, pp. 115–140. Elsevier (2018). https://doi.org/10.1016/b978-0-12-816136-4.00016-6